

# Chemical potentials of light flavor quarks from yield ratios of negative to positive particles in Au+Au collisions at RHIC

Ya-Qin Gao<sup>1,\*</sup>, Hai-Ling Lao<sup>2</sup>, Fu-Hu Liu<sup>2,†</sup>

<sup>1</sup>*Department of Physics, Taiyuan University of Science and Technology, Taiyuan, Shanxi 030024, China*

<sup>2</sup>*Institute of Theoretical Physics & State Key Laboratory of Quantum Optics and Quantum Optics Devices, Shanxi University, Taiyuan, Shanxi 030006, China*

**Abstract:** The transverse momentum spectra of  $\pi^-$ ,  $\pi^+$ ,  $K^-$ ,  $K^+$ ,  $\bar{p}$ , and  $p$  produced in Au+Au collisions at center-of-mass energy  $\sqrt{s_{NN}} = 7.7, 11.5, 19.6, 27, 39, 62.4, 130, \text{ and } 200$  GeV are analyzed in the framework of a multisource thermal model. The experimental data measured at midrapidity by the STAR Collaboration are fitted by the (two-component) standard distribution. The effective temperature of emission source increases obviously with the increase of the particle mass and the collision energy. At different collision energies, the chemical potentials of up, down, and strange quarks are obtained from the antiparticle to particle yield ratios in given transverse momentum ranges available in experiments. With the increase of logarithmic collision energy, the chemical potentials of light flavor quarks decrease exponentially.

**Keywords:** transverse momentum spectra; chemical potentials of quarks; standard distribution

**PACS** 25.75.-q, 24.10.Pa, 25.75.Dw

## 1 Introduction

The constructions of the Relativistic Heavy Ion Collider (RHIC) and the Large Hadron Collider (LHC) have been opening a new epoch for the studies of nuclear and quark matters. One of the major goals of the RHIC and LHC studies is to obtain information on the quantum chromodynamics (QCD) phase diagram [1]. The phase diagram includes at least a fundamental phase transition between the hadron gas and the quark-gluon plasma (QGP) or quark matter, and is usually plotted as chemical freeze-out temperature ( $T_{ch}$ ) versus baryon chemical potential ( $\mu_{baryon}$ ). Nowadays, the detailed characteristics of the phase diagram are not known yet. The experimental and theoretical nuclear physicists have been focusing their attentions on the searching for the critical end point and phase boundary. Lattice QCD calculations show that a system is produced at small  $\mu_{baryon}$  or high energies through a crossover at the quark-hadron phase transition [2, 3, 4]. Based on the lattice QCD [5] and several QCD-based models calculations [6, 7, 8, 9], as well as mathematical extensions of lattice techniques [10, 11, 12, 13], researchers suggest

that the transition at larger  $\mu_{baryon}$  is the first order and the QCD critical end point is existent.

Pinpointing the phase boundary and the critical end point is the central issue to understand the properties of interacting matter under extreme conditions and to map the QCD phase diagram. The matter produced in high-energy heavy-ion collisions provides the opportunity to search for the phase boundary and the critical end point [6, 14]. To this end, the STAR Collaboration at the RHIC has undertaken the first phase of the beam energy scan (BES) program [15, 16, 17], and starting the second phase from 2018 to 2019 [18]. The program is to vary the collision energy which enables a search for non-monotonic excitation functions over a broad domain of the phase diagram. Before looking for an evidence for the existence of a critical end point and the phase boundary, it is important to know the  $(T_{ch}, \mu_{baryon})$  region of phase diagram one can access. The produced particles spectra and yield ratios allow us only to infer the values of  $T_{ch}$  and  $\mu_{baryon}$  [19]. Furthermore, the bulk properties such as rapidity density  $dN/dy$ , mean transverse momentum  $\langle p_T \rangle$ , particle ratios, and freeze-out properties may provide an insight into the particle

\*E-mail: gyq610@163.com; gaoyaqin@tyust.edu.cn

†E-mail: fuhuliu@163.com; fuhuliu@sxu.edu.cn

production mechanisms at BES energies. Therefore, it is very important to study these bulk properties systematically, which may reveal the evolution and the changes of the system created in high-energy heavy-ion collisions.

As one of the most important measured quantities, the transverse momentum ( $p_T$ ) spectrum includes abundant information which are related to the excitation degree of the collision system. The spectra of identified particles can also provide useful information about temperature, particle ratio, and chemical potential by using thermal and statistical investigations [20]. For any system, one can determine the direction and limitation of mass transfer by comparing the chemical potentials of particles, that is to say that the chemical potential is a sign to mark the direction of spontaneous chemical reaction. The chemical potential can also be a criterion for determining whether thermodynamic equilibrium does exist in the interacting region in high-energy collisions [1]. Generally, a low absolute value of chemical potential corresponds to a high degree of thermodynamic equilibrium. Therefore, the chemical potential is also one of the major solutions for investigating the QGP. One can see that the chemical potentials of quarks are an important subject at high energy. Therefore, we are very interested in measurements the chemical potentials of quarks.

In this paper, we extract the chemical potentials of light flavor quarks from the yield ratios of negatively to positively charged particles. By using the (two-component) standard distribution, the  $p_T$  spectra of  $\pi^-$ ,  $\pi^+$ ,  $K^-$ ,  $K^+$ ,  $\bar{p}$ , and  $p$  produced in Au+Au collisions at center-of-mass energy (per nucleon pair)  $\sqrt{s_{NN}} = 7.7, 11.5, 19.6, 27, 39, 62.4, 130,$  and  $200$  GeV measured by the STAR Collaboration in midrapidity interval ( $|y| < 0.1$ ) [19, 21] are described. The considered energies stretch across a wide energy range which covers the main range of the RHIC at its BES.

## 2 The model and method

To extract the chemical potentials of quarks, we need to know the yield ratios of negatively to positively charged particles. Although we can have the values of yield ratios directly in experiments, they are not complete and comprehensive in some cases. Usually, the  $p_T$  spectra of charged particles are given in many experiments and we can get the yield ratios by fitting the

available data. Then, the values of chemical potentials for the up, down, and strange quarks can be obtained from the yield ratios  $\pi^-/\pi^+$ ,  $K^-/K^+$ , and  $\bar{p}/p$  which are synthetically considered in special ways.

In this paper, the  $p_T$  spectra are analyzed in the framework of a multisource thermal model [22], which assumes that various sources are involved in high-energy collisions. These sources are divided into few groups by different interaction mechanisms, geometrical relations, or event samples. Each group of sources forms a relatively large emission source which stays in a local thermal equilibrium state at the chemical or kinetic freeze-out. Each emission source is considered to emit particles in its rest frame and treated as a thermodynamic system of relativistic and quantum ideal gas. This means that each emission source can be described by the thermal and statistical model or other similar models and distributions. The final-state distribution is attributed to all sources in the whole system, which results in a multi-characteristic emission process [22] if we use the standard distribution [23, 24, 25, 26]. This also means that  $p_T$  spectrum can be described by a multi-component standard distribution in which each component describes a given emission source.

We now structure the multi-component standard distribution. It is assumed that there are  $l$  components to be considered. For the  $i$ -th component, the standard Boltzmann, Fermi-Dirac and Bose-Einstein distributions [23, 24, 25, 26] can be uniformly expressed as

$$f_i(p_T) = \frac{1}{N} \frac{dN}{dp_T} = C_i p_T \sqrt{p_T^2 + m_0^2} \int_{y_{\min}}^{y_{\max}} \cosh y \times \left[ \exp \left( \frac{\sqrt{p_T^2 + m_0^2} \cosh y - \mu}{T_i} \right) + S \right]^{-1} dy, \quad (1)$$

where  $C_i$  is the normalization constant which results in  $\int_0^\infty f_i(p_T) dp_T = 1$ ;  $N$ ,  $m_0$ ,  $\mu$ , and  $T_i$  denote the particle number, the rest mass of the considered particle, the chemical potential of the considered particle, and the effective temperature for the  $i$ -th component, respectively;  $y_{\min}$  is the minimum rapidity and  $y_{\max}$  is the maximum rapidity; the values of  $S$  are 0, +1, and -1, which denote the Boltzmann, Fermi-Dirac, and Bose-Einstein distributions, respectively. We neglect the existence of  $\mu$  in Eq. (1) due to the fact that it has mainly effect on the normalization which can be redone, but not the trend of curve.

In the final state,  $p_T$  spectrum is resulting from  $l$  components, that is

$$f(p_T) = \frac{1}{N} \frac{dN}{dp_T} = \sum_{i=1}^l w_i f_i(p_T), \quad (2)$$

where  $w_i$  ( $i = 1, 2, \dots, l$ ) is the relative weight resulting from the  $i$ -th component. Because of the probability distribution being acquiescently normalized to 1, the coefficient obeys the normalization condition of  $\sum w_i = 1$ . Considering the relative contribution of each component, we have the mean effective temperature to be  $T_{eff} = \sum w_i T_i$ , which reflects the mean excitation degree of different sources corresponding to different components and can be used to describe the effective temperature of whole interacting system. It should be noted that the effective temperature contains the contributions of transverse flow and thermal motion. It is not the “real” temperature of the interacting system.

According to Refs. [27, 28], the relation between antiproton to proton yield ratios can be written as

$$\frac{\bar{p}}{p} = \exp\left(-\frac{2\mu_p}{T_{ch}}\right) \approx \exp\left(-\frac{2\mu_{baryon}}{T_{ch}}\right), \quad (3)$$

where  $\mu_p$  denotes the chemical potential of proton. In the framework of the statistical thermal model of non-interacting gas particles with the assumption of standard Maxwell-Boltzmann statistics, there is an empirical expression for  $T_{ch}$  [29, 30, 31, 32], one has

$$T_{ch} = T_{lim} \frac{1}{1 + \exp[2.60 - \ln(\sqrt{s_{NN}})/0.45]}, \quad (4)$$

where  $\sqrt{s_{NN}}$  is in the units of GeV and the “limiting” temperature  $T_{lim} = 0.164$  GeV [29, 30].

In a similar way, the yield ratios of antiparticles to particles for other hadrons can be written as

$$\begin{aligned} k_\pi &\equiv \frac{\pi^-}{\pi^+} = \exp\left(-\frac{2\mu_\pi}{T_{ch}}\right), \\ k_K &\equiv \frac{K^-}{K^+} = \exp\left(-\frac{2\mu_K}{T_{ch}}\right), \\ k_p &\equiv \frac{\bar{p}}{p} = \exp\left(-\frac{2\mu_p}{T_{ch}}\right), \\ k_D &\equiv \frac{D^-}{D^+} = \exp\left(-\frac{2\mu_D}{T_{ch}}\right), \\ k_B &\equiv \frac{B^-}{B^+} = \exp\left(-\frac{2\mu_B}{T_{ch}}\right), \end{aligned} \quad (5)$$

where  $k_j$  ( $j = \pi, K, p, D, \text{ and } B$ ) denote the yield ratios of negatively to positively charged particles obtained from the normalization constants of  $p_T$  spectra.

The symbols  $\mu_\pi, \mu_K, \mu_D,$  and  $\mu_B$  represent the chemical potentials of  $\pi, K, D,$  and  $B,$  respectively. In the above discussion, the symbol of a given particle is used for its yield for the purpose of simplicity. Furthermore, we have

$$\begin{aligned} \mu_\pi &= -\frac{1}{2} T_{ch} \cdot \ln(k_\pi), \\ \mu_K &= -\frac{1}{2} T_{ch} \cdot \ln(k_K), \\ \mu_p &= -\frac{1}{2} T_{ch} \cdot \ln(k_p), \\ \mu_D &= -\frac{1}{2} T_{ch} \cdot \ln(k_D), \\ \mu_B &= -\frac{1}{2} T_{ch} \cdot \ln(k_B). \end{aligned} \quad (6)$$

Let  $\mu_q$  denote the chemical potential for quark flavor, where  $q = u, d, s, c,$  and  $b$  represent the up, down, strange, charm, and bottom quarks, respectively. In principle, we can use  $k_j$  to give relations among different  $\mu_q$ . The values of  $\mu_q$  are then expected from these relations. According to Refs. [33, 34], based on the same  $T_{ch}, k_j$  in terms of  $\mu_q$  are

$$\begin{aligned} k_\pi &= \exp\left[-\frac{(\mu_u - \mu_d)}{T_{ch}}\right] / \exp\left[\frac{(\mu_u - \mu_d)}{T_{ch}}\right] \\ &= \exp\left[-\frac{2(\mu_u - \mu_d)}{T_{ch}}\right], \\ k_K &= \exp\left[-\frac{(\mu_u - \mu_s)}{T_{ch}}\right] / \exp\left[\frac{(\mu_u - \mu_s)}{T_{ch}}\right] \\ &= \exp\left[-\frac{2(\mu_u - \mu_s)}{T_{ch}}\right], \\ k_p &= \exp\left[-\frac{(2\mu_u + \mu_d)}{T_{ch}}\right] / \exp\left[\frac{(2\mu_u + \mu_d)}{T_{ch}}\right] \\ &= \exp\left[-\frac{2(2\mu_u + \mu_d)}{T_{ch}}\right], \\ k_D &= \exp\left[-\frac{(\mu_c - \mu_d)}{T_{ch}}\right] / \exp\left[\frac{(\mu_c - \mu_d)}{T_{ch}}\right] \\ &= \exp\left[-\frac{2(\mu_c - \mu_d)}{T_{ch}}\right], \\ k_B &= \exp\left[-\frac{(\mu_u - \mu_b)}{T_{ch}}\right] / \exp\left[\frac{(\mu_u - \mu_b)}{T_{ch}}\right] \\ &= \exp\left[-\frac{2(\mu_u - \mu_b)}{T_{ch}}\right]. \end{aligned} \quad (7)$$

Thus, we have

$$\begin{aligned}
\mu_u &= -\frac{1}{6}T_{ch} \cdot \ln(k_\pi \cdot k_p), \\
\mu_d &= -\frac{1}{6}T_{ch} \cdot \ln(k_\pi^{-2} \cdot k_p), \\
\mu_s &= -\frac{1}{6}T_{ch} \cdot \ln(k_\pi \cdot k_K^{-3} \cdot k_p), \\
\mu_c &= -\frac{1}{6}T_{ch} \cdot \ln(k_\pi^{-2} \cdot k_p \cdot k_D^3), \\
\mu_b &= -\frac{1}{6}T_{ch} \cdot \ln(k_\pi \cdot k_p \cdot k_B^{-3}).
\end{aligned} \tag{8}$$

As can be seen from Eq. (8) that  $\mu_q$  are obtained from  $k_j$ . In addition to the yield ratios  $\pi^-/\pi^+$ ,  $K^-/K^+$  and  $\bar{p}/p$ , other combinations can also give  $\mu_q$  if the spectra in the numerator and denominator are under the same experimental conditions.

### 3 Results and discussion

The energy dependent double-differential  $p_T$  spectra of  $\pi^-$ ,  $\pi^+$ ,  $K^-$ ,  $K^+$ ,  $\bar{p}$ , and  $p$  produced in central Au+Au collisions at  $\sqrt{s_{NN}} = 7.7, 11.5, 19.6, 27, 39, 62.4, 130, \text{ and } 200$  GeV at the midrapidity  $|y| < 0.1$  are presented in Fig. 1, where the centrality interval at 130 GeV is 0–6% and at other energies is 0–5%. The different symbols represent the data measured by the STAR Collaboration [19, 21], and the curves are the results fitted here by the (two-component) standard distribution. Generally, the standard distribution is firstly used in the fit process. If it does not fit the data, the two-component standard distribution is used. It is because of the quality of the measurements that (two-component) standard distribution is used. In the case of using the two-component standard distribution, the first component results in narrow  $p_T$  region and the second component results in wide  $p_T$  regions. That is, in low  $p_T$  region both components contribute to the spectra, and in high  $p_T$  region only the second component contributes to the spectra. In the calculation, the values of the free parameters ( $T_1$ ,  $w_1$ , and  $T_2$ ), the normalization constant ( $N_0$ ), and  $\chi^2$  obtained by fitting the data are listed in Table 1 including the degrees of freedom (dof). One can see that the data are well fitted by the (two-component) standard distribution. From the parameter values, one

can see that the effective temperature increases with the increase of the particle mass and the collision energy for emissions of the six types of particles.

Based on the above successful fits of the  $p_T$  spectra of antiparticles and particles, we can use Eq. (8) and the  $p_T$  spectra in Fig. 1 to study the dependence of  $\mu_q$  on  $\sqrt{s_{NN}}$ . This is done by integrating the yield over the given  $p_T$  ranges available in experiments at different energies. Figure 2 shows the correlations between  $\mu_q$  and  $\sqrt{s_{NN}}$ , where  $\mu$  is used on the vertical axis to replace  $\mu_q$  which are marked in the panel for different styles of symbols. With the increase of logarithmic  $\sqrt{s_{NN}}$ , an exponential decrease of  $\mu_q$  is observed. Corresponding to the solid, dashed and dotted curves which fit to the dependences of  $\mu_u$ ,  $\mu_d$ , and  $\mu_s$  on  $\sqrt{s_{NN}}$ , respectively, we have

$$\begin{aligned}
\mu_u &= (820.1 \pm 0.1)(\sqrt{s_{NN}}[\text{GeV}])^{-(0.914 \pm 0.025)} \text{ MeV}, \\
\mu_d &= (681.1 \pm 0.1)(\sqrt{s_{NN}}[\text{GeV}])^{-(0.834 \pm 0.031)} \text{ MeV}, \\
\mu_s &= (420.7 \pm 0.2)(\sqrt{s_{NN}}[\text{GeV}])^{-(1.004 \pm 0.063)} \text{ MeV}
\end{aligned} \tag{9}$$

with the  $\chi^2/\text{dof} = 1.67/6, 2.73/6, \text{ and } 1.04/6$ , respectively.

The similarity in up and down quark masses renders the similarity in their chemical potentials. The difference between the chemical potentials of up (or down) and strange quarks is caused by the difference between their masses. At the lowest BES energy the difference between the chemical potentials are dozens of MeV, while at the highest RHIC energy these quantities are around a few MeV. The decrease in  $\mu_q$  is obvious, which indicates the change of mean free path of produced quarks in the middle state. If the produced quarks at the lowest BES energy have a small mean free path which looks as if a liquid-like middle state is formed, the produced quarks at the highest RHIC energy should have a large mean free path which looks as if a gas-like middle state is formed. The main difference at different energies is different mean free paths of the produced quarks. To search for the critical energy at which the change from a liquid-like middle state to a gas-like middle state had happen is beyond the focus of the present work.

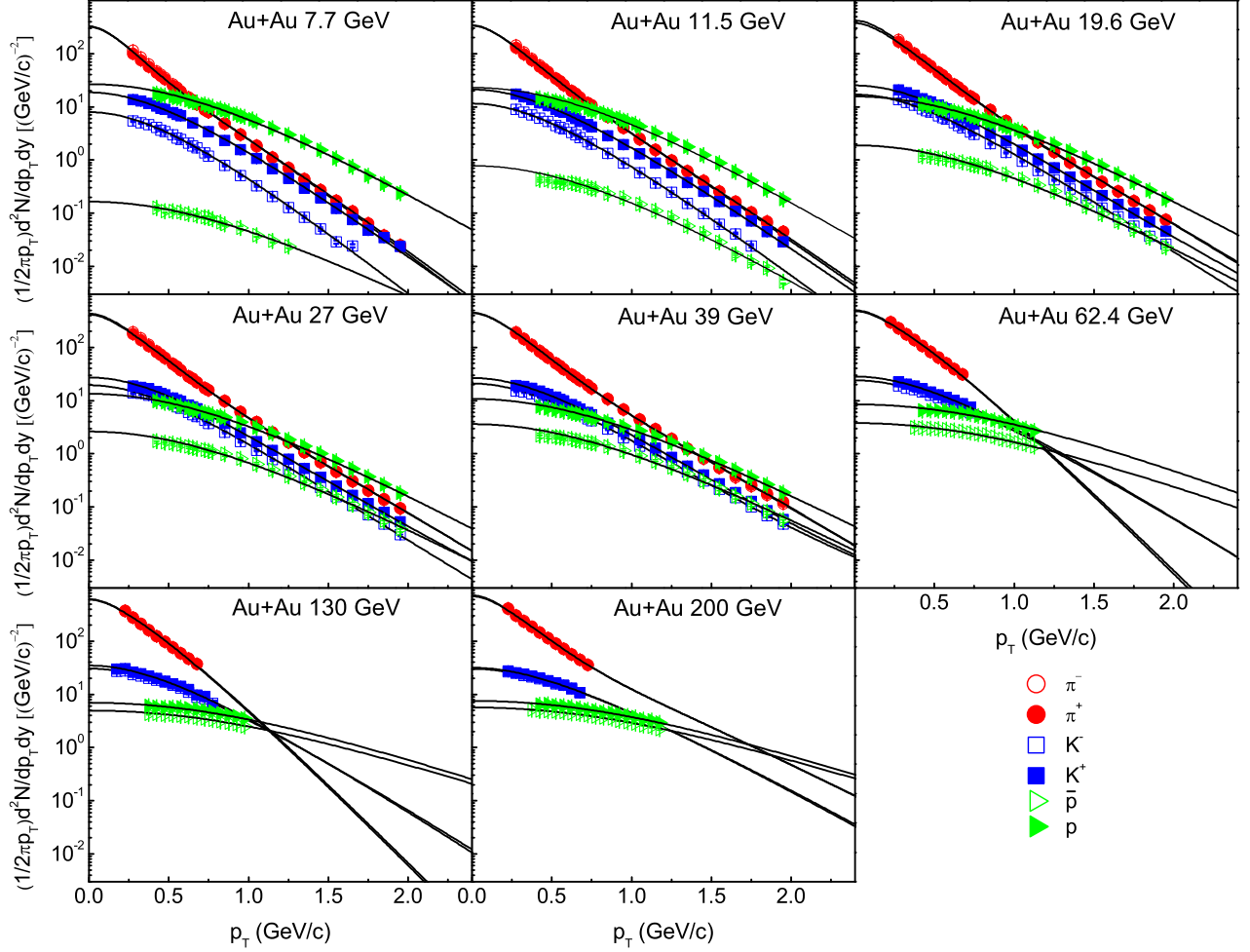


Fig. 1: Midrapidity ( $|y| < 0.1$ ) double-differential  $p_T$  spectra for  $\pi^-$ ,  $\pi^+$ ,  $K^-$ ,  $K^+$ ,  $\bar{p}$ , and  $p$  in central Au+Au collisions at  $\sqrt{s_{NN}} = 7.7, 11.5, 19.6, 27, 39, 62.4, 130,$  and  $200$  GeV, where the centrality interval at 130 GeV is 0–6% and at other energies is 0–5%. The different symbols represent the measurements done by the STAR experiment [19, 21] and the curves represent the results fitted by the (two-component) standard distribution. The values of parameters can be found in Table 1.

Table 1: Values of  $T_1$ ,  $w_1$ ,  $T_2$ ,  $N_0$ ,  $\chi^2$ , and dof corresponding to the curves in Fig. 1. The values for positively and negatively charged particles are given using the slash (/), where the values for positive particles are shown before the slash and the values for negative particles after the slash. The values of  $N_0$  are obtained due to the comparisons between the experimental  $(1/2\pi p_T)d^2N/dp_T dy$  and the calculated  $(1/2\pi p_T)N_0 f(p_T)/dy$ , where  $dy = 0.2$  and  $f(p_T)$  is presented in Eq. (2).

$\sqrt{s_{NN}}$ (GeV)	Particles	$T_1$ (MeV)	$w_1$	$T_2$ (MeV)	$N_0$	$\chi^2$	dof
7.7	$\pi^\pm$	$87 \pm 7/89 \pm 10$	$0.65 \pm 0.04/0.63 \pm 0.07$	$181 \pm 2/177 \pm 4$	$81.0 \pm 4.0/81.0 \pm 9.0$	$0.38/0.45$	22/22
	$K^\pm$	$185 \pm 6/170 \pm 8$	1.00/1.00	–	$9.5 \pm 0.8/3.8 \pm 0.5$	$0.75/0.98$	21/21
	$p/\bar{p}$	$224 \pm 7/257 \pm 20$	1.00/1.00	–	$19.0 \pm 0.2/0.13 \pm 0.01$	$1.15/0.52$	27/13
11.5	$\pi^\pm$	$102 \pm 10/105 \pm 10$	$0.70 \pm 0.04/0.69 \pm 0.03$	$193 \pm 4/190 \pm 4$	$92.0 \pm 8.0/93.0 \pm 8.0$	$0.25/0.48$	22/22
	$K^\pm$	$190 \pm 5/178 \pm 4$	1.00/1.00	–	$11.0 \pm 0.8/5.7 \pm 0.5$	$0.49/0.97$	23/21
	$p/\bar{p}$	$217 \pm 10/216 \pm 20$	1.00/1.00	–	$16.0 \pm 3.0/0.54 \pm 0.10$	$1.70/3.07$	26/21
19.6	$\pi^\pm$	$118 \pm 10/116 \pm 10$	$0.79 \pm 0.02/0.83 \pm 0.02$	$215 \pm 8/219 \pm 7$	$109.0 \pm 10.0/119.0 \pm 10.0$	$0.19/0.40$	22/22
	$K^\pm$	$181 \pm 7/181 \pm 5$	$0.88 \pm 0.04/0.89 \pm 0.05$	$260 \pm 20/239 \pm 20$	$13.0 \pm 1.4/8.7 \pm 0.8$	$0.55/1.61$	22/22
	$p/\bar{p}$	$234 \pm 20/237 \pm 10$	1.00/1.00	–	$11.5 \pm 2.0/1.4 \pm 0.1$	$0.69/19.81$	27/20
27	$\pi^\pm$	$117 \pm 8/118 \pm 7$	$0.79 \pm 0.03/0.81 \pm 0.03$	$219 \pm 7/221 \pm 7$	$120.0 \pm 10.0/125.0 \pm 10.0$	$0.19/0.27$	22/22
	$K^\pm$	$178 \pm 7/180 \pm 6$	$0.85 \pm 0.03/0.84 \pm 0.06$	$262 \pm 20/236 \pm 10$	$14.0 \pm 1.0/10.0 \pm 1.0$	$0.27/0.92$	22/21
	$p/\bar{p}$	$239 \pm 7/247 \pm 10$	1.00/1.00	–	$10.0 \pm 2.0/2.0 \pm 0.2$	$0.84/1.28$	21/20
39	$\pi^\pm$	$114 \pm 10/116 \pm 10$	$0.78 \pm 0.02/0.78 \pm 0.02$	$222 \pm 7/222 \pm 6$	$129.0 \pm 12.0/128.0 \pm 10.0$	$0.39/0.20$	22/22
	$K^\pm$	$189 \pm 7/189 \pm 5$	$0.95 \pm 0.01/0.96 \pm 0.02$	$332 \pm 18/347 \pm 23$	$14.0 \pm 1.5/11.0 \pm 1.0$	$0.20/0.36$	22/22
	$p/\bar{p}$	$250 \pm 20/252 \pm 20$	1.00/1.00	–	$8.3 \pm 1.0/2.8 \pm 0.3$	$0.81/2.42$	20/21
62.4	$\pi^\pm$	$139 \pm 6/137 \pm 8$	1.00/1.00	–	$146.0 \pm 10.0/150.0 \pm 10.0$	$1.14/1.07$	8/8
	$K^\pm$	$210 \pm 25/214 \pm 25$	1.00/1.00	–	$15.8 \pm 1.0/13.6 \pm 0.8$	$0.02/0.37$	8/8
	$p/\bar{p}$	$335 \pm 20/346 \pm 40$	1.00/1.00	–	$8.3 \pm 0.4/3.8 \pm 0.3$	$1.97/1.60$	13/14
130	$\pi^\pm$	$136 \pm 8/137 \pm 7$	1.00/1.00	–	$181.0 \pm 13.0/185.0 \pm 11.0$	$1.98/3.68$	8/8
	$K^\pm$	$204 \pm 12/210 \pm 13$	1.00/1.00	–	$18.5 \pm 1.4/17.3 \pm 1.3$	$0.39/0.20$	11/11
	$p/\bar{p}$	$373 \pm 15/385 \pm 22$	1.00/1.00	–	$7.5 \pm 0.7/5.5 \pm 0.3$	$1.73/0.47$	11/11
200	$\pi^\pm$	$116 \pm 8/115 \pm 5$	$0.76 \pm 0.03/0.76 \pm 0.03$	$263 \pm 23/262 \pm 25$	$209.0 \pm 14.0/215.0 \pm 12.0$	$0.21/0.17$	7/7
	$K^\pm$	$235 \pm 30/239 \pm 30$	1.00/1.00	–	$19.3 \pm 1.1/18.5 \pm 1.0$	$0.06/0.06$	8/8
	$p/\bar{p}$	$382 \pm 40/393 \pm 35$	1.00/1.00	–	$8.3 \pm 0.9/6.4 \pm 0.6$	$0.10/0.25$	14/15

From Eq. (9) we can obtain a linear relation between  $\ln \mu_q$  and  $\ln \sqrt{s_{NN}}$ ,

$$\ln \mu_q = a - |b| \cdot \ln \sqrt{s_{NN}}, \quad (10)$$

where the intercept  $a$  and slope  $-|b|$  can be obtained from the parameters in Eq. (9). In particular,  $-|b|$  is close to  $-1$ . The large negative slope shows an obvious anticorrelation between  $\ln \mu_q$  and  $\ln \sqrt{s_{NN}}$ . It is expected that  $\ln \mu_q$  will be smaller at higher energy or larger at lower energy. In particular, at the LHC energies,  $\ln \mu_q$  will be negative since  $\mu_q$  will be less than 1 MeV. The limiting value of  $\mu_q$  is close to 0 at the LHC [35], which results in an obvious negative  $\ln \mu_q$ .

The main conclusion observed from Fig. 2 is that  $\mu_q$  is high (from dozens of MeV to  $\sim 100$  MeV) at the BES and close to 0 at the LHC [35]. This is consistent with the trend of  $\mu_{baryon}$  ( $\sim 100$ – $300$  MeV at the BES and  $\sim 1$  MeV at the LHC) obtained from other works [1, 29, 30, 31, 32, 36]. This is natural due to the fact that baryon is consisted of valence quarks. If we regard  $\mu_{baryon} = \Sigma \mu_q$ , where  $\Sigma$  denotes the sum over all valence quarks in baryon, the present work is consistent with the models which study  $\mu_{baryon}$  [1, 29, 30, 31, 32, 36].

We would like to point out that although we have used the (two-component) standard distribution in the fits of  $p_T$  spectra and  $T_1$  ( $T_2$ ) has been used, the values of  $\mu_q$  obtained by us are independent of models and parameters. In fact,  $\mu_q$  is only related to  $k_j$  if  $T_{ch}$  is known. We can use directly the yield ratios of data to obtain  $\mu_q$ . The reason why we use the function form instead of data is to extend  $p_T$  spectrum in intermediate region to low and high regions where the data are not available. In our opinion, the function fitted the data in intermediate  $p_T$  region can predict approximately the trends in low and high  $p_T$  regions.

## 4 Conclusions

In summary, we found a good fit of the transverse momentum spectra of charged particles produced in central Au+Au collisions at the RHIC at its BES energies. It is shown that the (two-component) standard distribution successfully fitted the data measured at midrapidity by the STAR Collaboration, though other distributions

are also acceptable. The effective temperature parameter increases with the increase of the particle mass and the collision energy.

At BES energies, the chemical potentials of light flavor quarks were obtained from the yield ratios of negatively to positively charged particles in given transverse momentum ranges available in experiments. At low energy, the chemical potentials of up and down quarks are consistent but differ from that of strange quark. At high energy, the three chemical potentials seem to deviate from each other, and they finally approach zero at very high energy.

From the lowest BES energy to the highest RHIC energy, with the increase of logarithmic collision energy, an exponential decrease of the chemical potentials of light flavor quarks is observed. The similarity in up and down quark masses renders the similarity in their chemical potentials. The difference between the chemical potentials of up (or down) and strange quarks is caused by their different masses. The difference between the chemical potentials changes from dozens of MeV to a few MeV. The decrease in chemical potential indicates that the mean free path of produced quarks changes from a small value to a large one.

### Data Availability

All data are quoted from the mentioned references. As a phenomenological work, this paper does not report new data.

### Conflicts of Interest

The authors declare that there are no conflicts of interest regarding the publication of this paper.

### Acknowledgments

Communications from Edward K. Sarkisyan-Grinbaum are highly acknowledged. This work was supported by the National Natural Science Foundation of China under Grant Nos. 11747063, 11575103, and 11747319, the Doctoral Scientific Research Foundation of Taiyuan University of Science and Technology under Grant No. 20152043, the Shanxi Provincial Natural Science Foundation under Grant No. 201701D121005, and the Fund for Shanxi “1331 Project” Key Subjects Construction.

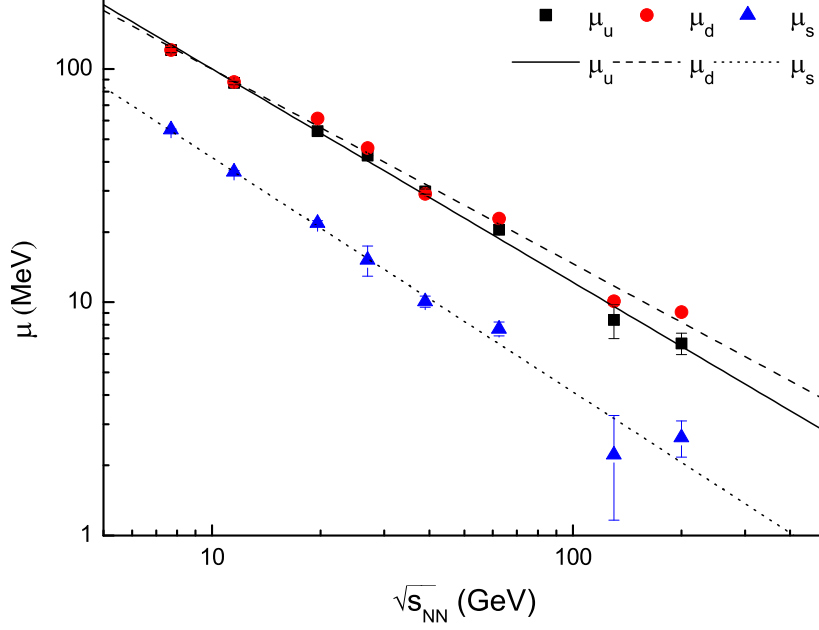


Fig. 2: Correlations between  $\mu_q$  and  $\sqrt{s_{NN}}$  for central Au+Au collisions at RHIC. The symbols represent  $\mu_q$  obtained from the ratios by integrating the yield over the given  $p_T$  ranges available in experiments in Fig. 1. The solid, dashed and dotted curves are fitted results corresponding to  $\mu_u$ ,  $\mu_d$  and  $\mu_s$ , respectively.

## References

- [1] P. Braun-Munzinger, J. Wambach, Rev. Mod. Phys. **81**, 1031 (2009).
- [2] Y. Aoki, G. Endrodi, Z. Fodor, S. Katz, K. Szabo, Nature (London) **443**, 675 (2006).
- [3] T. Bhattacharya et al. (HotQCD Collaboration), Phys. Rev. Lett. **113**, 082001 (2014).
- [4] M. Cheng, N. H. Christ, S. Datta et al., Phys. Rev. D **77**, 014511 (2008).
- [5] S. Ejiri, Phys. Rev. D **78**, 074507 (2008).
- [6] M. Asakawa, K. Yazaki, Nucl. Phys. A **504**, 668 (1989).
- [7] A. Barducci, R. Casalbuoni, S. De Curtis, R. Gatto, G. Pettini, Phys. Lett. B **231**, 463 (1989).
- [8] A. Barducci, R. Casalbuoni, S. De Curtis, R. Gatto, G. Pettini, Phys. Rev. D **41**, 1610 (1990).
- [9] M. A. Stephanov, Prog. Theor. Phys. Suppl. **153**, 139 (2004).
- [10] Z. Fodor, S. Katz, J. High Energy Phys. **04**, 050 (2004).
- [11] A. Li, A. Alexandru, K.-F. Liu, Phys. Rev. D **84**, 071503 (2011).
- [12] K. Nagata, K. Kashiwa, A. Nakamura, S. M. Nishigaki, Phys. Rev. D **91**, 094507 (2015).
- [13] P. de Forcrand, J. Langelage, O. Philipsen, W. Unger, Phys. Rev. Lett. **113**, 152002 (2014).
- [14] M. A. Stephanov, K. Rajagopal, E. V. Shuryak, Phys. Rev. Lett. **81**, 4816 (1998).
- [15] B. I. Abelev et al. (STAR Collaboration), Phys. Rev. C **81**, 024911 (2010).
- [16] L. Kumar, Nucl. Phys. A **904**, 256c (2013).
- [17] L. Kumar, Mod. Phys. Lett. A **28**, 1330033 (2013).
- [18] <https://drupal.star.bnl.gov/STAR/starnotes/public/sn0670>
- [19] L. Adamczyk et al. (STAR Collaboration), Phys. Rev. C **96**, 044904 (2017).
- [20] P. Braun-Munzinger, I. Heppe, J. Stachel, Phys. Lett. B **465**, 15 (1999).
- [21] B. I. Abelev et al., (STAR Collaboration), Phys. Rev. C **79**, 034909 (2009).
- [22] F.-H. Liu, Nucl. Phys. A **810**, 159 (2008).
- [23] J. L. Synge, *The Relativistic Gas* (North-Holland, Amsterdam, The Netherlands, 1957).
- [24] P. Z. Ning, L. Li, D. F. Min, *Foundation of Nuclear Physics: Nucleons and Nuclei* (Higher Education Press, Beijing, China, 2003).
- [25] C. D. Dermer, Astrophys. J. **280**, 328 (1984).
- [26] J. Cleymans, D. Worku, Eur. Phys. J. A **48**, 160 (2012).
- [27] P. Braun-Munzinger, D. Magestro, K. Redlich, J. Stachel, Phys. Lett. B **518**, 41 (2001).
- [28] S. S. Adler et al. (PHENIX Collaboration), Phys. Rev. C **69**, 034909 (2004).

- [29] A. Andronic, P. Braun-Munzinger, J. Stachel, *Acta Phys. Pol. B* **40**, 1005 (2009).
- [30] A. Andronic, P. Braun-Munzinger, J. Stachel, *Nucl. Phys. A* **834**, 237c (2010).
- [31] A. Andronic, P. Braun-Munzinger, J. Stachel, *Nucl. Phys. A* **772**, 167 (2006).
- [32] J. Cleymans, H. Oeschler, K. Redlich, S. Wheaton, *Phys. Rev. C* **73**, 034905 (2006).
- [33] I. Arsene et al. (BRAHMS Collaboration), *Nucl. Phys. A* **757**, 1 (2005).
- [34] H. Zhao, F.-H. Liu, *Adv. High Energy Phys.* **2015**, 137058 (2015).
- [35] H.-L. Lao, Y.-Q. Gao, F.-H. Liu, arXiv:1806.04309 [hep-ph] (2018).
- [36] J. Rafelski, *Eur. Phys. J. A* **51**, 114 (2015).